Chapter 3.

Phase Transformations in a

$Cu_{2.7}Mn_{0.3}Al$ Alloy

Phase Transformations in a $Cu_{2.7}Mn_{0.3}Al$ Alloy

Abstract

The as-quenched microstructure of the $Cu_{2.7}Mn_{0.3}Al$ alloy was $D0_3$ phase containing extremely fine L-J precipitates. When the as-quenched alloy was aged at 500℃ for moderate times, the L-J precipitates started to appear at the regions contiguous to the γ-brass particles. The coexistence of (γ-brass + L-J) phases has never been observed by other workers in the Cu-Mn-Al alloy systems before. When the as-quenched alloy was aged at temperatures ranging from 500℃ to 700℃, the phase transition sequence was found to be (γ-brass + L-J + $D0_3$) → (γ-brass + L-J + B2) → β. This result is different from that reported by previous workers in $Cu_{3-x}Mn_xAl$ alloys with $X \leq 0.32$.

3-1 Introduction

In previous studies, it is seen that when an alloy with a chemical composition in the range of $Cu_{3-x}Mn_xAl$ with $X \leq 0.32$ was solution heat- treated in single β phase (disordered body-centered cubic) region and then quenched into ice brine rapidly, a β → B2 → $D0_3$ phase transition occurred during quenching [1-3]. When the as-quenched alloys were aged at temperatures ranging from 350℃ to 600℃, γ-brass particles were found to appear within the $D0_3$ or B2 matrix [4-6]. The γ-brass has a $D8_3$ (ordered body-centered cubic) structure with lattice parameter a=0.872 nm [7-9], and the orientation relationship between the γ-brass and the matrix was cubic to cubic [10-12]. Based on their studies, it is seen that the stable microstructure of the $Cu_{3-x}Mn_xAl$ alloys with $X \leq 0.32$ as the aging temperature increased changed from (γ-brass + $D0_3$) → (γ-brass + B2) → β.

Recently, we made transmission electron microscopy (TEM) observations on the phase transformations of the $Cu_{2.7}Mn_{0.3}Al$ alloy. Consequently, it was found that in the as-quenched condition, the microstructure of the alloy was $D0_3$ phase containing extremely fine L-J precipitates. The L-J phase is a new type of precipitate, which was firstly observed and identified by Liu and Jeng (designated L-J phase) in a $Cu_{2.2}Mn_{0.8}Al$ alloy, which has an orthorhombic structure with lattice parameters a=0.413nm, b=0.254nm and c=0.728nm [13]. When the as-quenched alloy was aged at temperatures ranging from 500℃ to 700℃, the phase transition sequence was found to be (γ-brass + L-J + $D0_3$) → (γ-brass + L-J + B2) → β, rather than (γ-brass + $D0_3$) → (γ-brass + B2) → β

reported by previous workers in $Cu_{3-x}Mn_xAl$ alloy with $X \leq 0.32$.

3-2 Experimental procedure

The alloy, $Cu_{2.7}Mn_{0.3}Al$ (Cu-7.6at.%Mn-25.1at.%Al), was prepared in a vacuum induction furnace by using 99.9% Cu, 99.9% Al and 99.9% Mn. The melt was chill cast into a 30x50x200-mm copper mold. After being homogenized at 900℃ for 72 hours, the ingot was sectioned into 2.0-mm thick slices. These slices were subsequently solution heat-treated at 900℃ for 1 hour and then quenched into room-temperature water rapidly. The aging processes were performed at temperatures ranging from 500℃ to 700℃ for various times in a vacuum heat-treated furnace and then quenched rapidly.

TEM specimens were prepared by means of a double-jet electropolisher with an electrolyte of 70% methanol and 30% nitric acid. The polishing temperature was kept in the range from -30℃ to -15℃, and the current density was kept in the range from $3.0x10^4$ to $4.0x10^4$ A/m^2. Electron microscopy was performed on a JEOL JEM-2000FX scanning transmission electron microscope operating at 200 KV. This microscope was equipped with a Link ISIS 300 energy-dispersive X-ray spectrometer (EDS) for chemical analysis. Quantitative analyses of elemental concentrations for Cu, Al and Mn were made with the aid of a Cliff-Lorimer Ratio Thin Section method.

3-3 Results and discussion

Figure 3.1(a) is a bright-field (BF) electron micrograph of the as-quenched alloy, exhibiting that a high density of extremely fine precipitates was formed within the matrix. Figures 3.1(b) and (c) are two selected-area diffraction patterns (SADPs) of the as-quenched alloy. It is seen in these SADPs that in addition to the reflection spots corresponding to the $D0_3$ phase [14-15], the diffraction patterns also consist of extra spots with streaks caused by the presence of the extremely fine precipitates. When compared with our previous studies in $Cu_{2.2}Mn_{0.8}Al$ and Cu-14.6Al-4.3Ni alloys [13, 16], it is found that these extra spots with streaks should belong to the L-J phase with two variants. Figure 3.1(d) is a $(\bar{1}11)$ $D0_3$ dark-field (DF) electron micrograph of the same area as Figure 1(a), revealing the presence of the fine $D0_3$ domains with a/2<100> anti-phase boundaries (APBs). Figure 3.1(e), a (002) $D0_3$ DF electron micrograph, shows the presence of the small B2 domains with a/4<111> APBs. In Figures 3.1(d) and (e), it is seen that the sizes of both $D0_3$ and B2 domains are very small. Therefore, it is deduced that the $D0_3$ phase existing in the as-quenched alloy was formed by a β → B2 → $D0_3$ continuous ordering transition during quenching [17-18]. Figure 3.1(f) is a (100_1) L-J DF electron micrograph, exhibiting the presence of the extremely fine L-J precipitates. Based on the above observations, it is concluded that the as-quenched microstructure of the alloy was $D0_3$ phase containing extremely fine L-J precipitates, where the $D0_3$ phase was formed by the β → B2 → $D0_3$ continuous ordering transition during quenching.

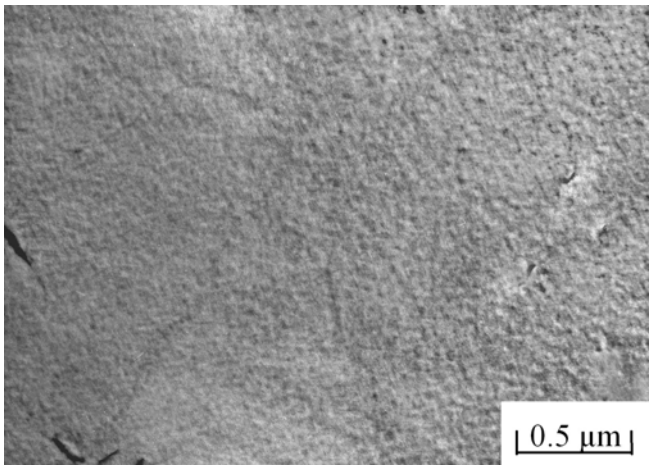

Figure 3.1(a)

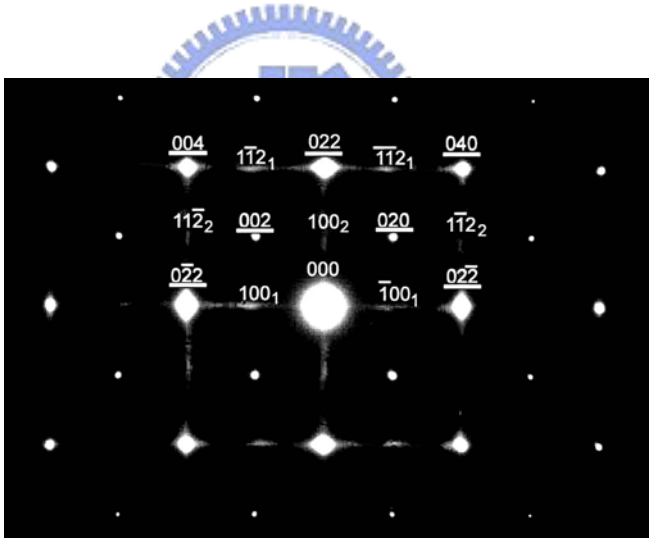

Figure 3.1 (b)

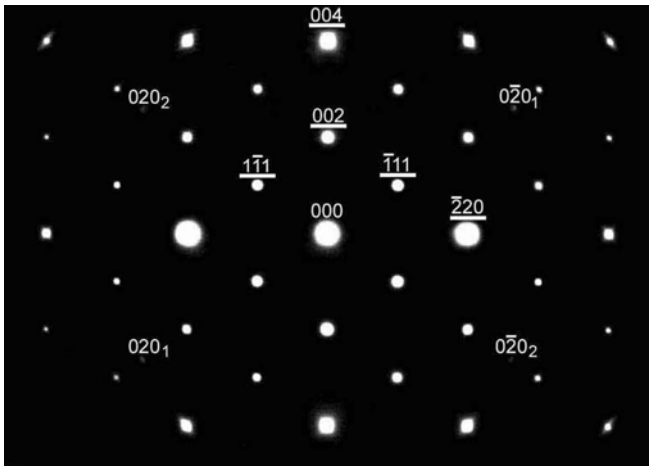

Figure 3.1(c)

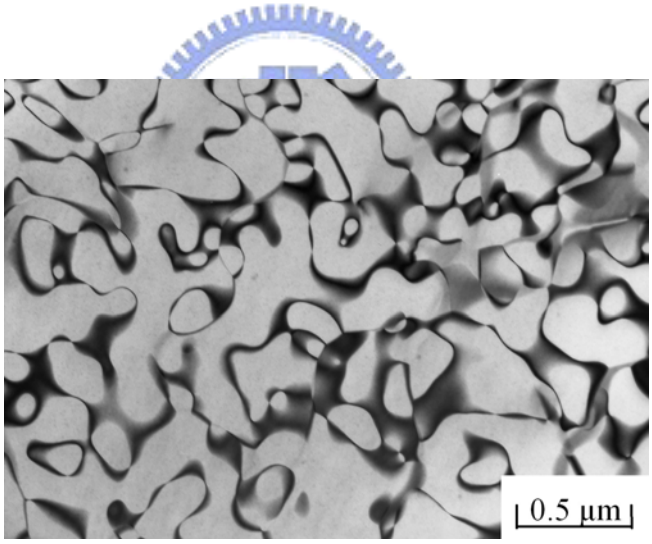

Figure 3.1 (d)

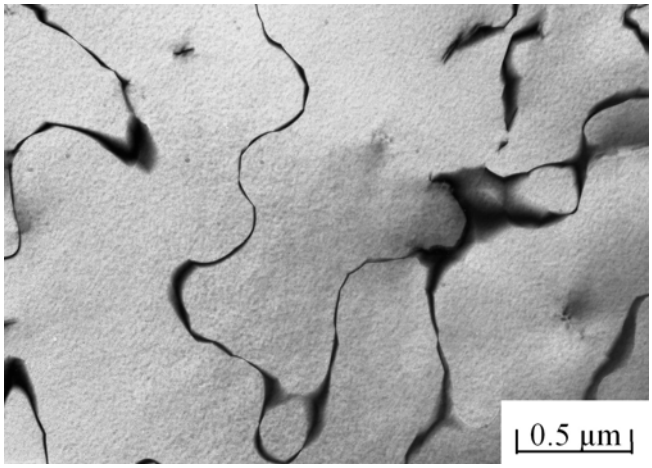

Figure 3.1(e)

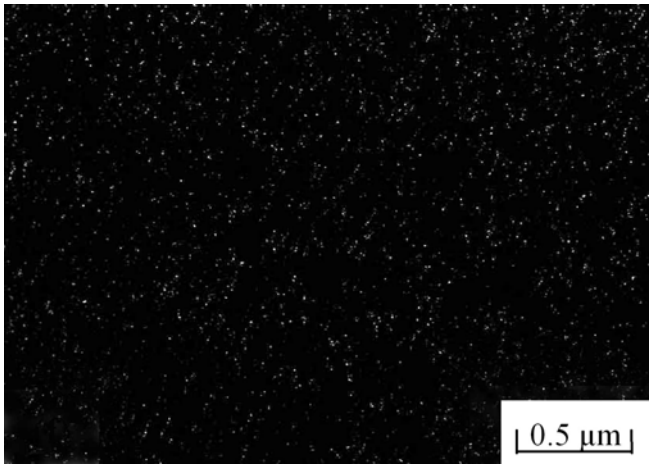

Figure 3.1 (f)

Figure 3.1 Electron micrographs of the as-quenched alloy. (a) BF, (b) and (c) two SADPs. The zone axes of the $D0_3$ phase are (b) $[100]$ and (c) $[110]$, respectively (<u>hkl</u>= $D0_3$, $hkl_{1,2}$= L-J phase, 1: variant 1; 2:variant 2), (d) and (e) $(\bar{1}11)$ and (002) $D0_3$ DF, respectively. (f) $(0\bar{2}0_1)$ L-J DF.

When the as-quenched alloy was aged at 500℃ for moderate times, some coarse particles with a cubic shape started to occur. A typical example is shown in Figure 3.2. Figure 3.2(a) shows a BF electron micrograph of the alloy aged at 500℃ for 20 minutes. Electron diffraction demonstrated that the cubic-shaped particles were of γ-brass phase. Figures 3.2(b) and (c) are two SADP taken from an area covering the particle marked as "R" in Figure 3.2(a) and its surrounding matrix. It indicates that the orientation relationship between the γ-brass and the $D0_3$ matrix is $(001)_{\gamma\text{-brass}}$ //$(001)_m$ and $(010)_{\gamma\text{-brass}}$ //$(010)_m$, which is similar to that found by previous workers in Cu-Al based alloys [10-12]. Figure 3.2(d), a $(\bar{1}11)$ $D0_3$ DF electron micrograph of the same area as Figure 3.2(a), exhibits that the $D0_3$ domains had grown considerably and that the a/2<100> APBs were gradually disappeared. In Figure 3.2(d), it is also seen that the γ-brass particles occurred preferentially at a/2<100> APBs. Shown in Figure 3.2(e) is a $(0\bar{2}0_1)$ L-J DF electron micrograph, revealing that after being aged at 500℃ for 20 minutes, the size of the L-J precipitates was increased significantly, that is, the L-J precipitates grew considerably. Figure 3.2(f) is a (100) γ-brass DF electron micrograph, clearly showing the presence of the cubic-shaped γ-brass particles within the $D0_3$ matrix. With increasing the aging time at 500℃, the γ-brass particles grew rapidly and the morphology would changes from cubic to irregular shape, as illustrated in Figure 3.3(a). Figures 3.3(b) and (C) are two SADPs taken from a region marked as "A" in Figure 3.3(a), indicating that the intensity of the reflection spots and streaking behavior of the L-J precipitates increased with increasing the aging time.

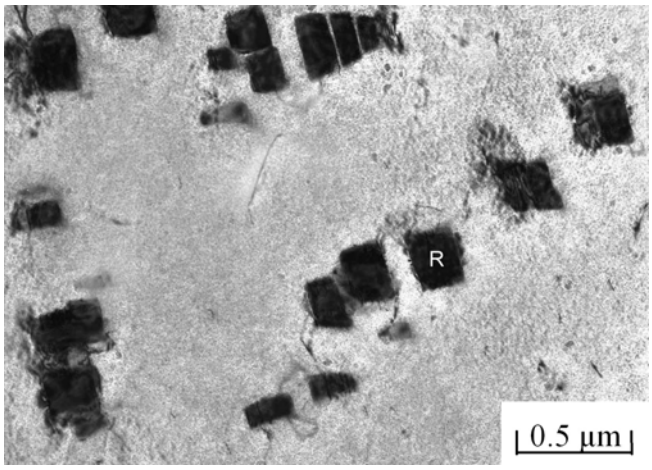

Figure 3.2(a)

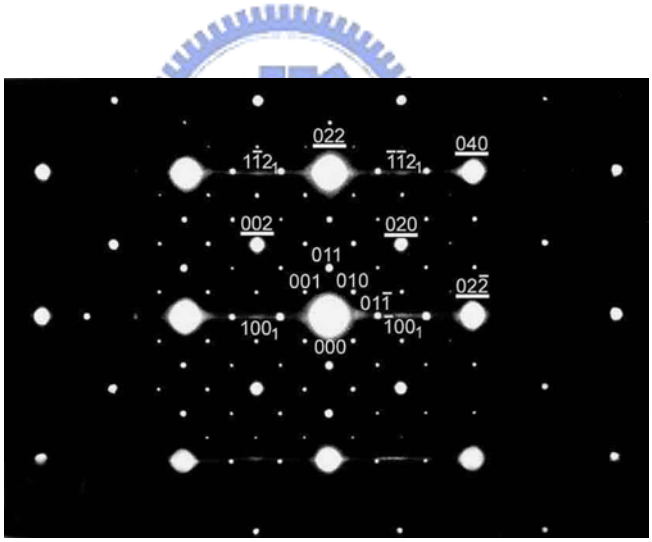

Figure 3.2 (b)

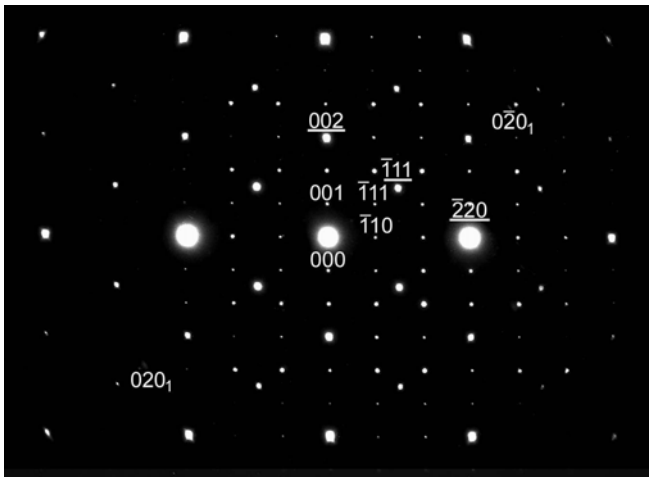

Figure 3.2(c)

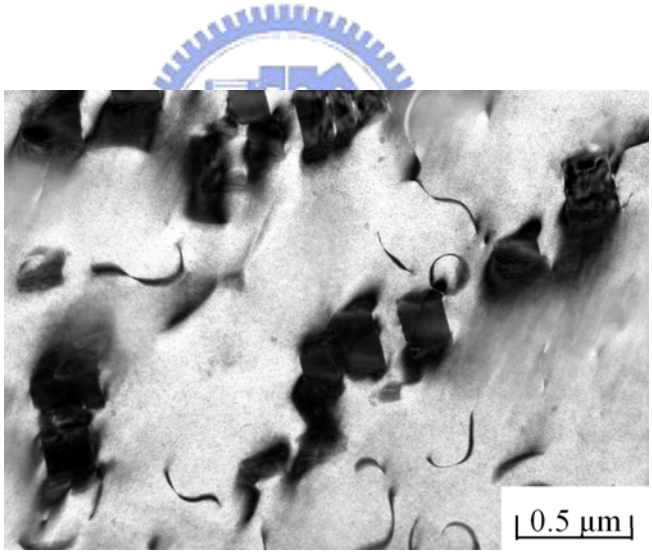

Figure 3.2 (d)

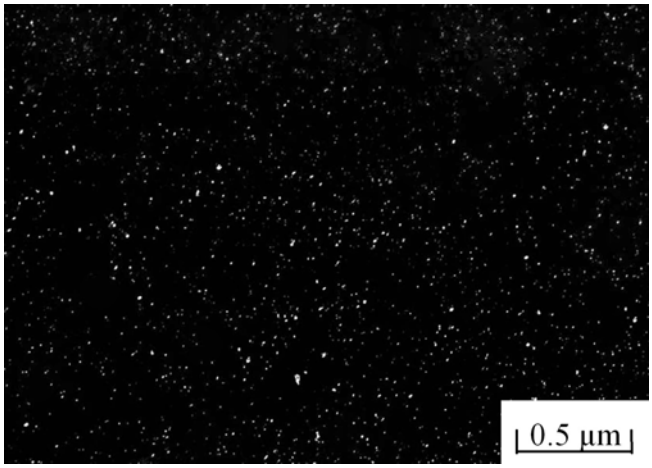

Figure 3.2 (e)

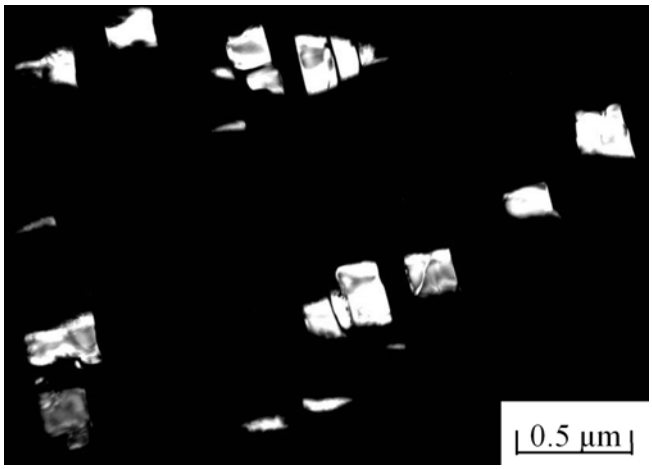

Figure 3.2 (f)

Figure 3.2 Electron micrographs of the alloy aged at 500 ℃ for 20 minutes. (a) BF, (b) and (c) two SADPs. The zone axes of the $D0_3$ phase is $[100]$ and $[110]$, respectively. (hkl=$D0_3$, hkl_1=L-J phase and hkl=γ-brass), (c) and (d) $(\bar{1}11)$ $D0_3$ and (100_1) L-J DF, respectively. (f) (100) γ-brass DF.

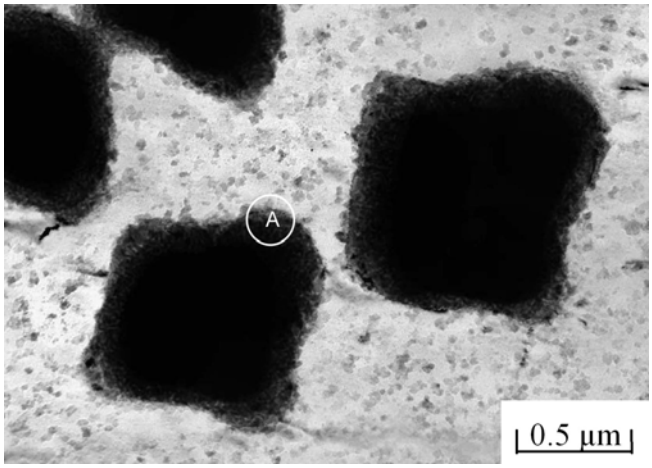

Figure 3.3(a)

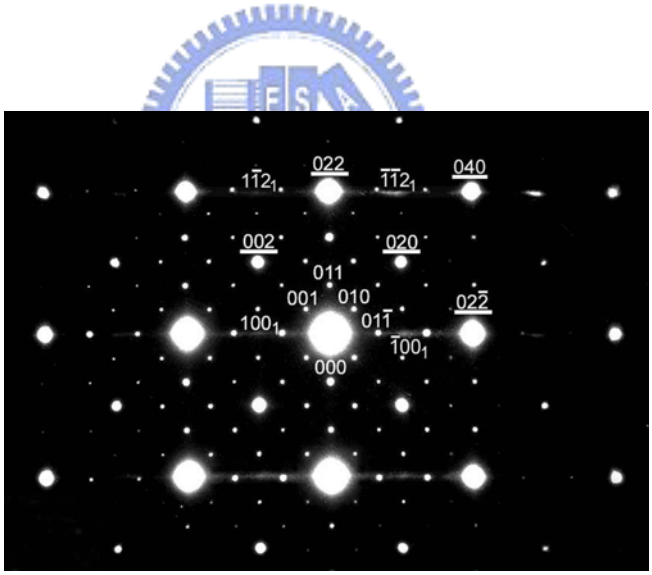

Figure 3.3 (b)

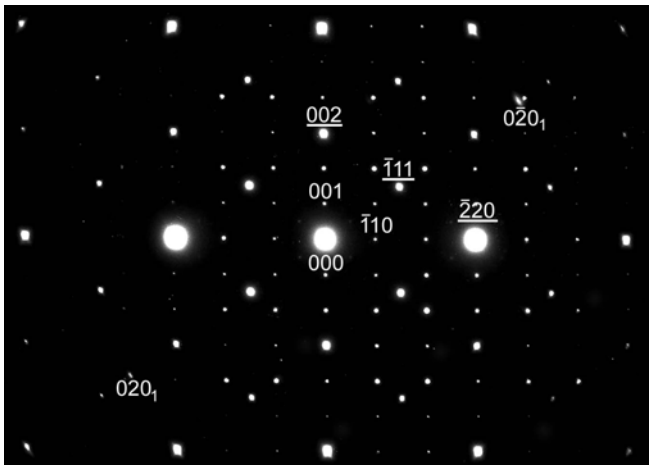

Figure 3.3(c)

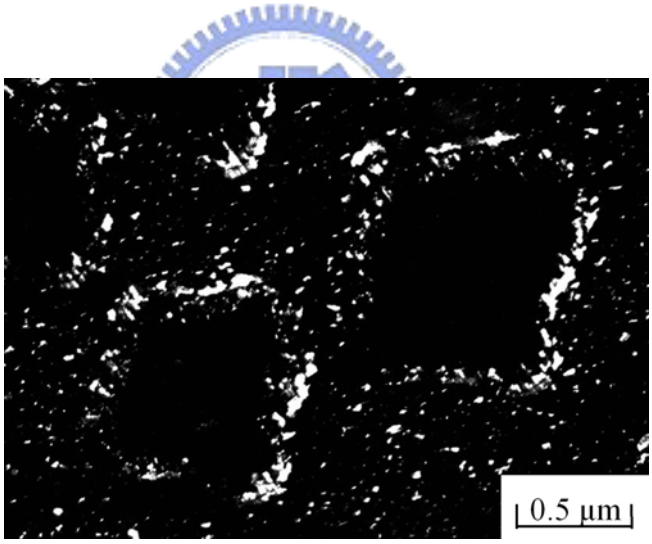

Figure 3.3 (d)

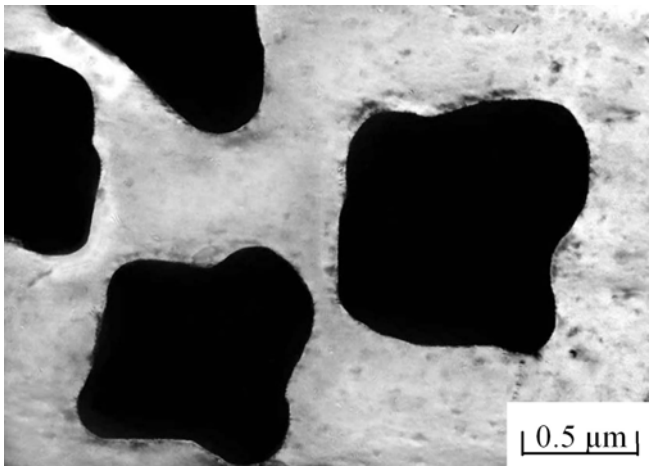

Figure 3.3 (e)

Figure 3.3 Electron micrographs of the alloy aged at 500℃ for 2 hours. (a) BF, (b) and (c) two SADPs. The zone axes of the $D0_3$ phase are $[100]$ and $[110]$. (<u>hkl</u>=$D0_3$, hkl_1=L-J phase and hkl=γ-brass), respectively. (d) and (e) (100_1) L-J and $(\bar{1}11)$ $D0_3$ DF, respectively.

Figure 3.3(d), a (100_1) L-J DF electron micrograph, reveals that the L-J precipitates grew considerably and the L-J precipitates surrounding the γ-brass particles were much larger than those away from γ-brass particles. Figure 3.3(e) shows a $(\bar{1}11)$ $D0_3$ DF electron micrograph, exhibiting that the $D0_3$ domains have grown to reach a complete grain. Apparently, the microstructure of the alloy present at 500℃ was a mixture of (γ-brass + L-J + $D0_3$) phases. It is noted here that the coexistence of the (γ-brass + L-J) phases has never been observed by previous workers in the Cu-Mn-Al alloy systems before.

Shown in Figure 3.4(a) is a BF electron micrograph of the alloy aged at 600℃ for 1 hour and then quenched, revealing the presence of the irregular-shaped particles. Figures 3.4(b) and (c) are two SADPs taken from the γ-brass particle and the $D0_3$ matrix, respectively. In these SADPs, it is found that the irregular-shaped particle is of the γ-brass phase and the matrix is a mixture of ($D0_3$ + L-J) phases. Figure 3.4(d) is a $(0\bar{2}0_1)$ L-J DF electron micrograph, indicating that the coexistence of (γ-brass + L-J) phases could also be observed. However, it is clearly seen in Figure 3.4 (d) that two types of L-J precipitates could be detected; one is the larger L-J precipitates surrounding the γ-brass particles which were existent at the aging temperature, and the other is the extremely fine L-J precipitates (the size being comparable to that observed in the as-quenched alloy) which were formed during quenching from the quenching temperature. Figures 3.4(e) and (f) show $(\bar{1}11)$ and (002) $D0_3$ DF electron micrographs, clearly exhibiting that the small quenched-in $D0_3$

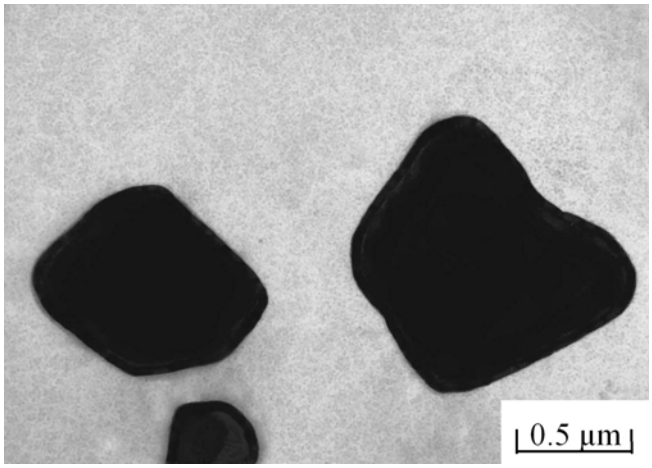

Figure 3.4(a)

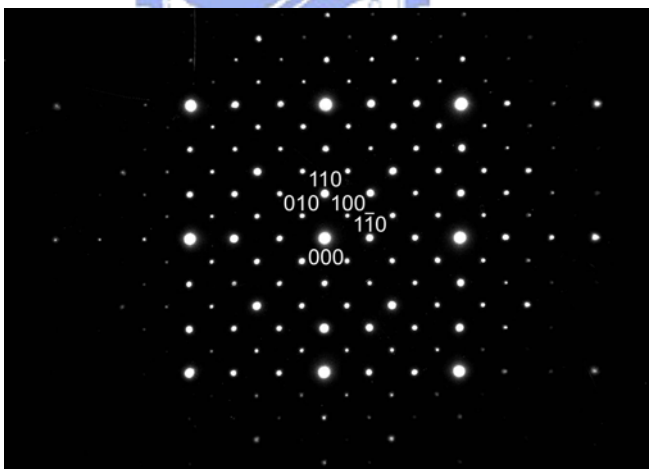

Figure 3.4 (b)

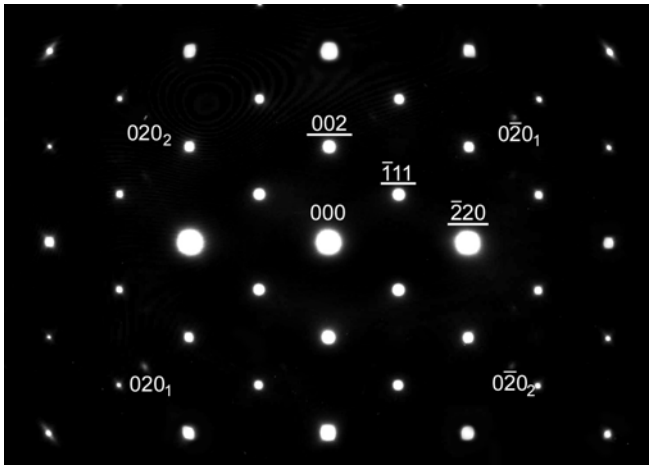

Figure 3.4(c)

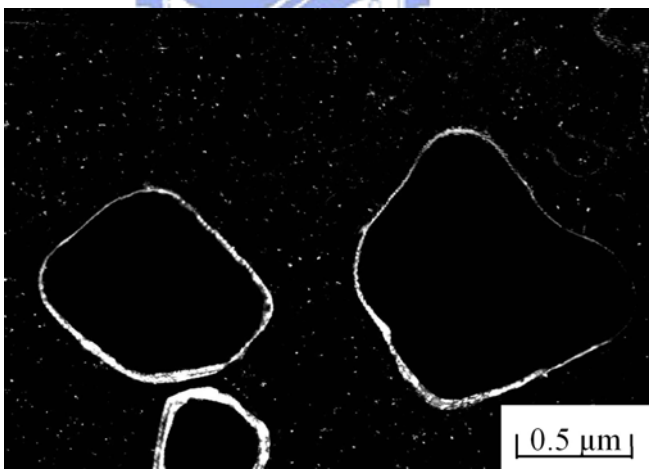

Figure 3.4 (d)

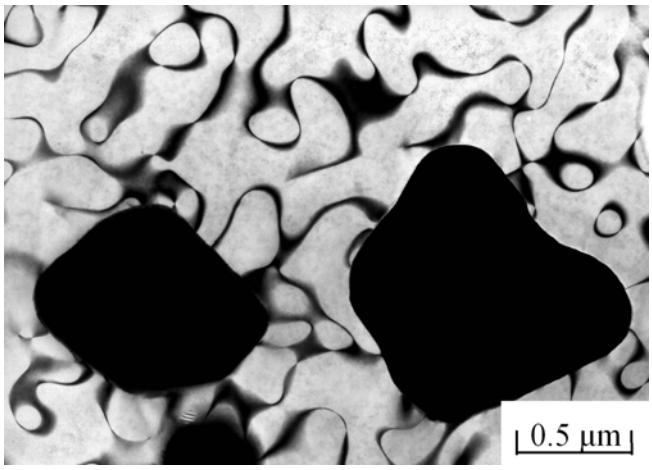

Figure 3.4(e)

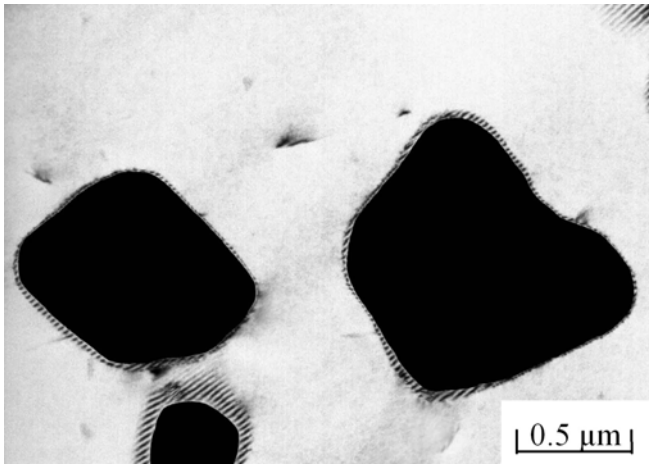

Figure 3.4 (f)

Figure 3.4 Electron micrographs of the alloy aged at 600 ℃ for 1 hour. (a) BF, (b) an SADP take from the irregular-shaped γ-brass particle. The zone axis of the γ-brass phase is $[001]$. (c) an SADP taken from the $D0_3$ matrix. The zone axis of the $D0_3$ phase is $[110]$. (hkl=$D0_3$, hkl_1=L-J phase). (d) $(0\bar{2}0_1)$ L-J DF. (e) and (f) $(\bar{1}11)$ and (002) $D0_3$ DF, respectively.

domains and well-grown B2 domains, respectively. This indicates that the microstructure of the alloy present at 600℃ was a mixture of (γ-brass + L-J + B2) phases.

Progressively higher temperature aging and quenching experiments indicated that the mixture of (γ-brass + L-J + B2) was preserved up to 675℃. However, when the alloy was aged at 700℃ for 1 hour and then quenched, the microstructure is similar to that observed in the as-quenched alloy, as shown in Figure 3.5. This indicates that the microstructure existing at 700℃ or above is the single disordered β phase.

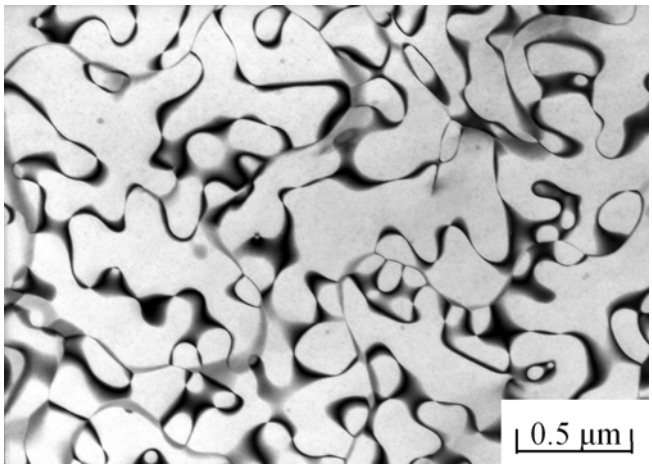

Figure 3.5(a)

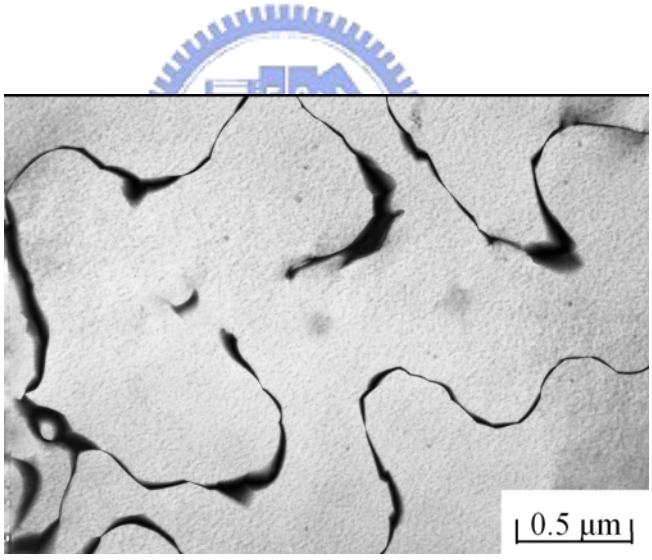

Figure 3.5 (b)

Figure 3.5 Electron micrographs of the alloy aged at 700 ℃ for 1 hour. (a) and (b) ($\bar{1}11$) and (002) $D0_3$ DF, respectively.

Based on the preceding results, it is obvious that the as-quenched microstructure of the present alloy was $D0_3$ phase containing extremely fine L-J precipitates. This is different from that examined by other workers in the $Cu_{3-x}Mn_xAl$ alloys with $X \leq 0.32$, in which they reported that the as-quenched microstructure was single $D0_3$ phase [1-3]. Here, it is worthwhile to point out that the extremely fine L-J precipitates had also been detected and identified by the present workers in the as-quenched $Cu_{2.2}Mn_{0.8}Al$ and Cu_2MnAl alloys [13, 19]. However, comparing to our previous studies, it is clear that the amount of the L-J precipitates existing in the present alloy is less than that observed in the previous alloys. It seems to imply that the higher Mn content in the $Cu_{3-x}Mn_xAl$ alloys may enhance the formation of the extremely fine L-J precipitates within the matrix during quenching.

The coexistence of (γ-brass + L-J) phases is a remarkable feature in the present study, which has never been observed by other workers in the Cu-Mn-Al alloy systems before. In order to clarify this feature, an STEM-EDS study was performed. Figures 3.6(a) through (c) represent three typical EDS spectra taken from the as-quenched alloy, a γ-brass particle and an L-J precipitate in the alloy aged at 500℃ for 2 hours, respectively. The average atomic percentages of alloy elements examined by analyzing at least ten different EDS spectra of each phase are listed in Table 3.1. In Table 3.1, the quantitative analyses revealed that the atomic percentage of the alloying elements in the γ-brass particle and L-J precipitate were Cu-2.76at.% Mn-29.84at.%Al and Cu-15.34at.%Mn-17.52at.%Al, respectively. It is clearly seen that the concentration of Mn in the γ-brass is much less than that in the

as-quenched alloy. Therefore, it is expected that along with the growth of γ-brass particles, the surrounding regions would be enriched in Mn. The enrichment in Mn would cause the Mn-rich L-J precipitates to form at the regions contiguous to the γ-brass particles, as observed in Figures 3.3(d) and 3.4(d).

Finally, it is worthwhile to note that when the alloy was aged at 500℃ for moderate times, γ-brass particles started to occur preferentially at a/2<100> APBs. This feature is similar to that observed by N. Zárubová et al. in an aged Cu-4.6wt.%Al-4.1wt.%Ni alloy [20].

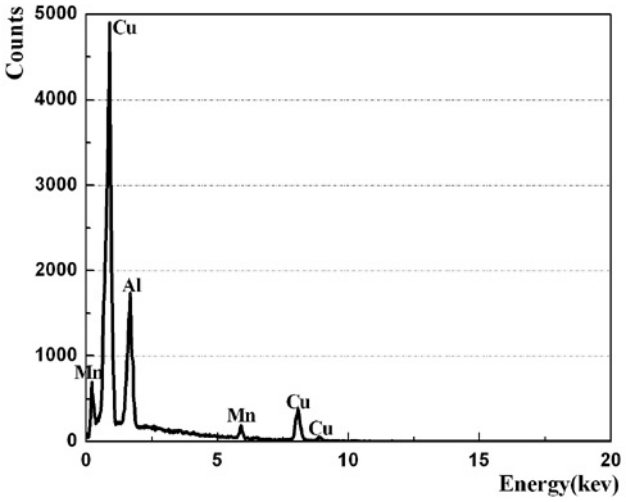

Figure 3.6(a)

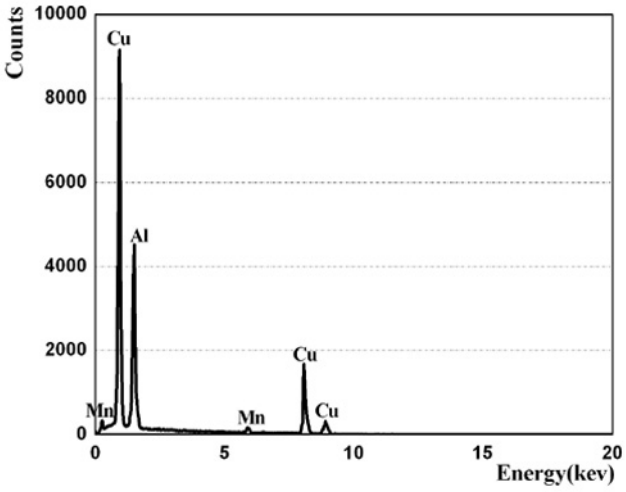

Figure 3.6 (b)

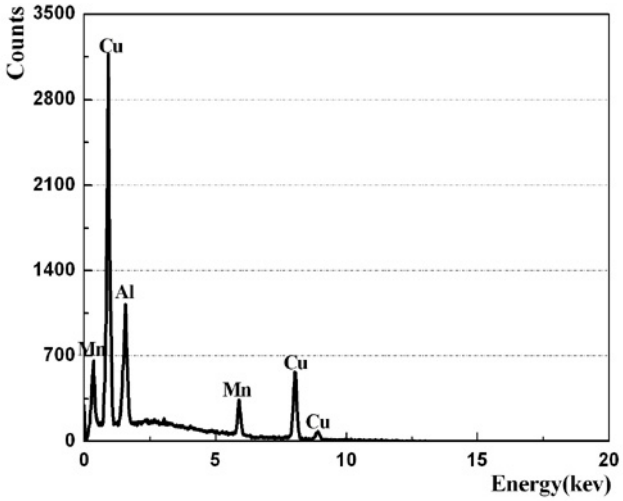

Figure 3.6(a)

Figure 3.6 Three typical EDS spectra obtained from (a) as-quenched alloy, (b) a γ-brass particle, and (c) an L-J precipitate in the alloy aged at 500℃ for 2 hours, respectively.

Table 3.1 Chemical Compositions of the Phases Revealed by an Energy-Dispersive X-ray Spectrometer (EDS)

Heat Treatment	Phase	Chemical Compositions (at.%)		
		Cu	Mn	Al
As-quenched	$D0_3$+ L-J	67.32	7.56	25.08
500℃, 2hrs	γ-brass	67.40	2.76	29.84
	L-J	67.14	15.34	17.52

3-4 Conclusions

The phase transformations in the $Cu_{2.7}Mn_{0.3}Al$ alloy have been studied by using transmission electron microscopy and energy–dispersive X-ray spectrometry.

1. In the as-quenched condition, the microstructure of the $Cu_{2.7}Mn_{0.3}Al$ alloy was $D0_3$ phase containing extremely fine L-J precipitates, where the $D0_3$ phase was formed by the $\beta \rightarrow B2 \rightarrow D0_3$ continuous ordering transition during quenching.

2. When the as-quenched alloy was aged at 500℃ for moderate times, the γ-brass particles were found to occur preferentially at a/2<100> APBs. With increasing aging time, the L-J precipitates started to appear at the regions contiguous to the γ-brass particles. The coexistence of (γ-brass + L-J) phases has never been observed by other workers in the Cu-Mn-Al alloy systems before.

3. The phase transition sequence as the aging temperature increased from 500℃ to 700℃ was found to be ($D0_3$ + L-J + γ-brass) → (B2 + L-J + γ-brass) → β.

References

1. J. Marcos, E. Vives, T. Castán: Phys. Rev. B 63 (2001) 224418.
2. R. Kainuma, N. Satoh, X. J. Liu, I. Ohnuma, K. Ishida: J. Alloy. Compd. 266 (1998) 191.
3. M. Prado, M. Sade, F. Lovey: Scrpita Metall. Mater. 28 (1993) 545.
4. E. Obradó, C. Frontera, L. Maoñsa, A. Planes: Phys. Rev. B 58 (1998) 14245.
5. J. J. Counioux, J. L. Macqueron, M. Robin, J. M. Scarabello: Scrpita Metall. 22 (1988) 821.
6. J. Miettinen. Calphad: 27 (2003) 103.
7. B. Dubois, D. Chevereau: J. Mater. Sci. 14 (1979) 2296.
8. M. A. Dvorack, N. Kuwano, S. Polat, H. Chen, C. M. Wayman: Scripta Metall. 17 (1983) 1333.
9. R. Kozubski, J. Soltys: J. Mater. Sci. 17 (1982) 1441.
10. J. Singh, H. Chen, C. M. Wayman: Scripta Metall. 19 (1985) 887.
11. R. Kozubski. J. Solty, J. Dutkiewicz, J. Morgiel: J. Mater. Sci. 22 (1987) 3843.
12. J. Dutkiewicz, J. Pons, E. Cesari: Mater. Sci. Eng. A 158 (1992) 119.
13. S. C. Jeng, T. F. Liu: Metall. Mater. Trans. A 26 (1995) 1353.
14. N. Kuwano, C. M. Wayman: Meatll. Trans. A 15 (1984) 621.
15. C. C. Wu, J. S. Chou, T. F. Liu: Meatll. Trans. A 22 (1991) 2265.
16. J. Tan, T. F. Liu: Mater. Chem. Phys. 70 (2001) 49.
17. P. R. Swann, W. R. Duff, R. M. Fisher: Metall Trans 3 (1972) 409.

18. S. M. Allen, J. W. Chan: Acta Metall. 24 (1976) 425.

19. K. C. Chu, T. F. Liu: Metall. Mater. Trans. A 30 (1999) 1705.

20. N. Zárubová, A. Gemperle, V. Novák: Mater. Sci. Eng. A 222 (1997) 166.